Electronic Supplementary Information

Zeolite-templated carbon-supported Ru-based catalysts for efficient alkaline hydrogen evolution reaction

Xin Wang,[a] Xiaoli Yang,*[b] Junwei Sun,[a] Mingyu Guo,[b] Zhihao Cao,[b] Haoxi Ben,[b] Wei Jiang,[b] Shujun Ming,[c] and Lixue Zhang*[a]

[a] College of Chemistry and Chemical Engineering, Collaborative Innovation Center for Hydrogen Energy Key Materials and Technologies of Shandong Province, Qingdao University, Qingdao 266071, China

[b] State Key Laboratory of Bio-Fibers and Eco-Textiles, Qingdao University, Qingdao 266071, China

[c] Hubei Key Laboratory of Processing and Application of Catalytic materials，Huanggang Normal University, Hubei 438000, China

* E-mail: xlyang@qdu.edu.cn (X. Yang); zhanglx@qdu.edu.cn (L. Zhang).

Experimental Section

Chemicals

All chemicals were of analytical grade and used without further purification. LaY zeolite was purchased from Nanjing University. HF and HCl were bought from Sinopharm Chemical Reagent Corp. $RuCl_3$ $3H_2O$ was purchased from Macklin Chemical Reagent Co., Ltd. Nafion (5 wt%) was purchased from Aladdin Chemical Reagent Co., Ltd. Ultrapure water (18.2 MΩ) was used in all experiments.

Synthesis of Catalysts.

The zeolite-template carbon (ZTC) was synthesized by chemical vapor deposition of ethylene gas on LaY zeolite. Typically, 2 g of LaY zeolite was heated to 600 ºC (80 mL min^{-1}, 5 ºC min^{-1}) under dry N_2 flow. Then ethylene/N_2/vapor mixed gas with a flow rate of 80 mL min^{-1} was introduced into the reactor for 90 min. Next, the sample was heated to 850 ºC (5 ºC min^{-1}) and maintained for 2 h under dry N_2 flow (80 mL min^{-1}). After cooling to room temperature, the obtained carbon/zeolite composite was etched with an aqueous HF/HCl solution to remove the zeolite template. The ZTC sample was collected by filtration, thoroughly washed with deionized water, and dried at 60 ºC overnight.

Ru/ZTCs and Pt/ZTCs were prepared via a conventional wet-impregnation method, followed by H_2 reduction. In a typical procedure, 0.1 g of the carbon support was dispersed into the appropriate amount of $RuCl_3$/H_2PtCl_6 solution (0.16mg mL^{-1} noble metal, the theoretical Ru/Pt loading amount was 5 wt%, the specific content was determined by Inductive Coupled Plasma Emission Spectrometer test, as shown in Table S1). After stirring continuously at room temperature for 2 h, the suspension was then stirred at 80 ºC for 6 h until dry. Then the samples were reduced at 300 ℃ (5 ºC min^{-1}) for 2 h under 10 vol% H_2/Ar (40 mL min^{-1}), expressed as Ru/ZTCs-300 and Pt/ZTCs-300, respectively. Similarly, Ru/ZTCs-200, Ru/ZTCs-400, and Ru/ZTCs-500 samples were prepared by changing the reduction temperature. For comparison, other Ru/carbon materials were synthesized via the same procedure with Ru/ZTCs-300.

Characterization

Powder X-ray diffraction (XRD) patterns were employed on a Bruker D8 Advance (Bruker AXS, Germany) X-ray diffractometer with Cu Kα radiation (40 kV 100 mA) of λ = 1.5418 Å at room

temperature, scanning speed: 10 ºC min^{-1}, and 2θ range of 5-85°. Surface area and pore structure were examined by Brunauer–Emmett–Teller and Barrett–Joyner–Halenda methods using an ASAP 2460-4HD surface area analyzer (Micromeritics Instrument). Scanning electron microscope (SEM) analysis was performed on a sigma500 (Cari Zeiss, Germany) scanning electron microscope at an accelerating voltage of 20 kV. Transmission electron microscope (TEM) measurements were conducted on a JEM-2100F (JEOL, Tokyo, Japan) electron microscope. Raman spectra were collected using a Thermo Scientific DXR2 Raman spectrometer (Thermo Fisher, America) with an excitation wavelength of 532 nm. X-ray photoelectron spectroscopy (XPS) experiments were carried out on an ESCALAB Xi+ X-ray photoelectron spectrometer using Mg as the exciting source. As a reference, the binding energy was corrected using the C 1s peak of the advantageous C peak at 284.8 eV.

XAS data at the Ru K-edge (including EXAFS and XANES) were acquired at the BL11B beamlines at the Shanghai Synchrotron Radiation Facility (SSRF) (Shanghai, China). Before the analysis at the beamline, samples were pressed into thin sheets with 1 cm in diameter and sealed using Kapton tape film. The XAFS spectra were recorded at room temperature using a 4-channel Silicon Drift Detector (SDD) Bruker 5040. Ru K-edge extended X-ray absorption fine structure (EXAFS) spectra were recorded in transmission mode. Negligible changes in the line-shape and peak position of Ru K-edge XANES spectra were observed between two scans taken for a specific sample. The spectra were processed and analyzed by the software codes Athena and Artemis.

Temperature-programmed desorption of hydrogen (H_2-TPD) experiment was carried out on an AutoChen1 II 2920 instrument. Before the test, the samples were pre-reduced at different temperatures

for 2 h under a flow of 10 vol% H_2/Ar (50 mL min^{-1}), followed by purging with high-purity argon for 30 min. After cooling to 50 °C, a 10% H_2/Ar mixture was injected into the reactor repeatedly until H_2 adsorption was saturated. Then the samples were heated at a rate of 10 ºC min^{-1} to 800 ºC under the Ar flow (20 mL min^{-1}). The amount of desorbed hydrogen was measured by a TCD detector.

Electrochemical Analysis.

All electrocatalytic measurements were performed on a Bio-logic VSP 300 electrochemical workstation with a three-electrode cell at room temperature. A graphite rod, a Hg/HgO reference electrode and a glassy carbon electrode (GCE, a diameter of 3 mm) modified with the electrocatalysts were used as the auxiliary electrode, the reference electrode and the working electrode, respectively.

To prepare the electrocatalyst electrode, 4 mg catalyst powder and 30 μL of Nafion solution were ultrasonically dispersed into 0.97 mL isopropanol. Then the suspension was sonicated for 30 min to get a homogeneous ink. Then, 5 μL of the catalyst ink was loaded onto the surface of the GCE and dried at room temperature.

The HER catalytic activity was measured in alkaline electrolytes (1 M KOH). Linear sweep voltammetry (LSV) measurements were performed with a scan rate of 10 mV s^{-1}. All polarization curves were without iR-compensated. Electrochemical impedance spectroscopy (EIS) measurements were carried out with frequencies range from 1 M Hz to 100 mHz with an AC amplitude of 5 mV. The double layer capacitance (C_{dl}) was measured from the CV curves at different scan rates (20, 40, 60, 80 and 100 mV s^{-1}), tested in non-Faradic potential range of -0.15– -0.05 V (vs Hg/HgO) by the formula: $ic = v \times C_{dl}$. Chronopotentiometry measurements were performed at current densities of 10 mA cm^{-2} to determine

the stability of the catalyst. All of the measured potentials of the electrocatalysts were referenced to the reversible hydrogen electrode (RHE) as follows:

$$E(RHE) = E(Hg/HgO) + (0.059 * pH) + 0.924$$

Supporting Figures

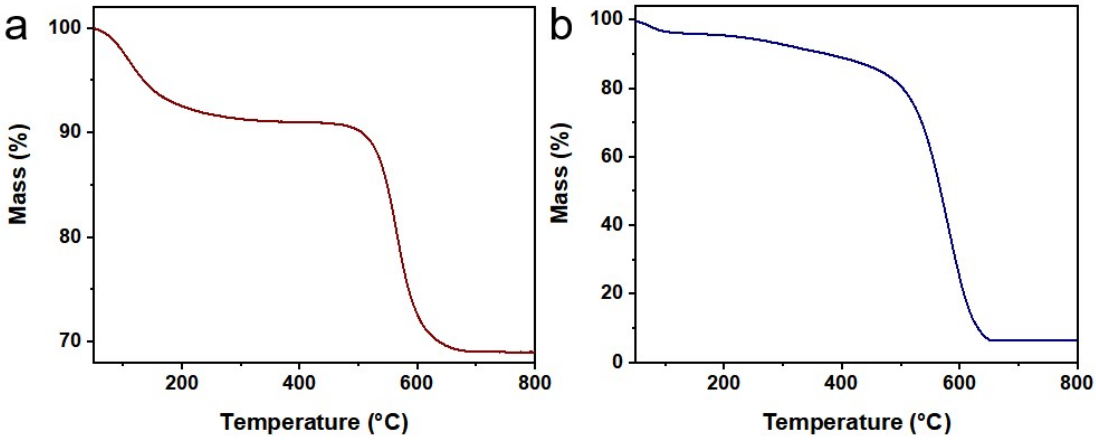

Figure S1. TGA curves of (a) LaY+ZTCs, (b) ZTCs.

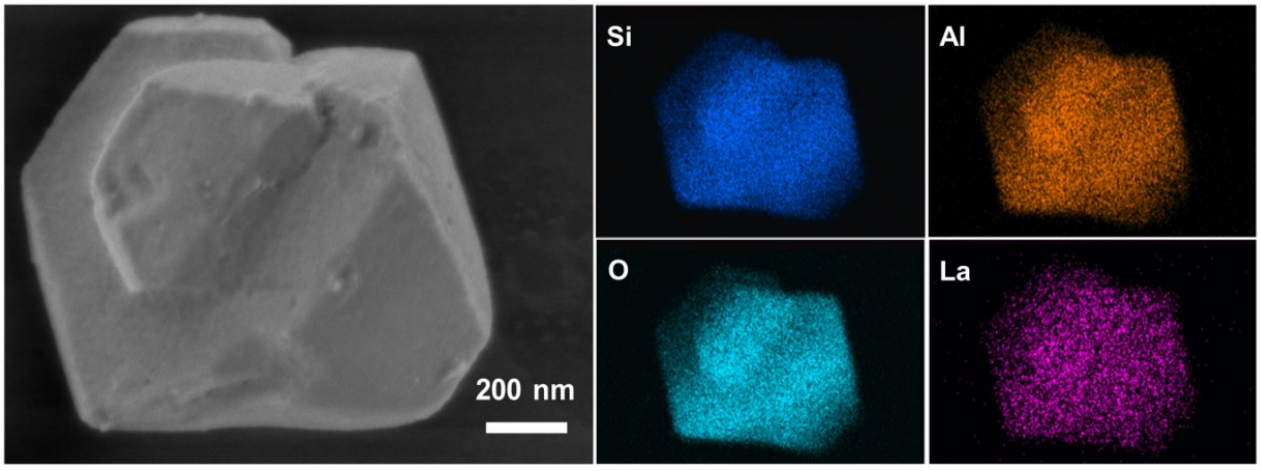

Figure S2. SEM and corresponding elemental mapping images of LaY zeolite.

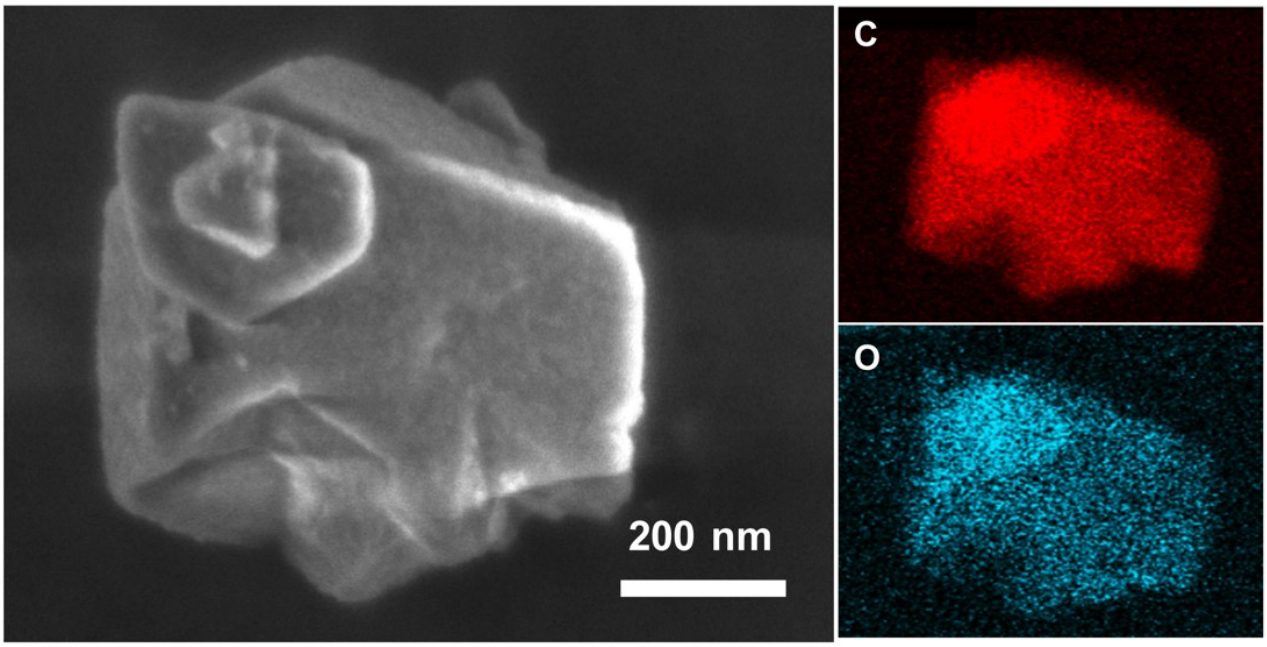

Figure S3. SEM and corresponding elemental mapping images of ZTCs.

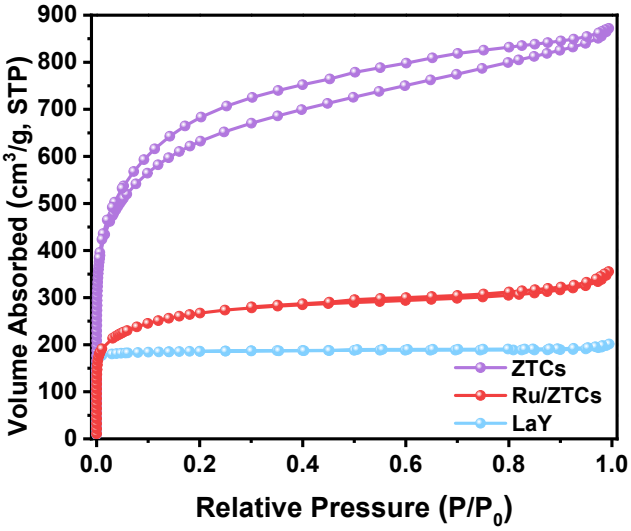

Figure S4. N_2 adsorption-desorption isotherms of LaY zeolite, ZTCs, and Ru/ZTCs-300.

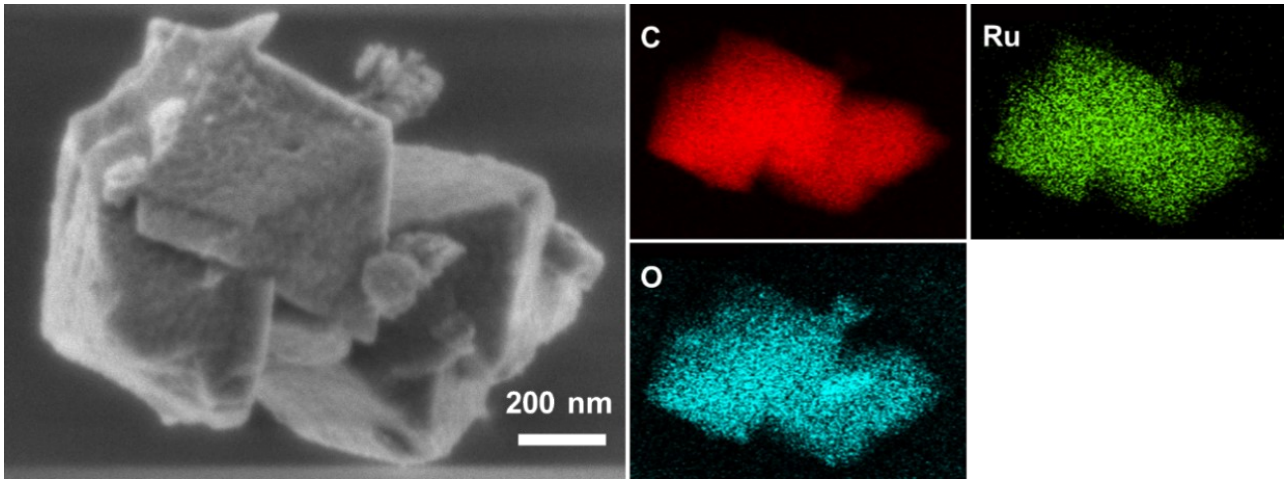

Figure S5. SEM and corresponding elemental mapping images of Ru/ZTCs-300.

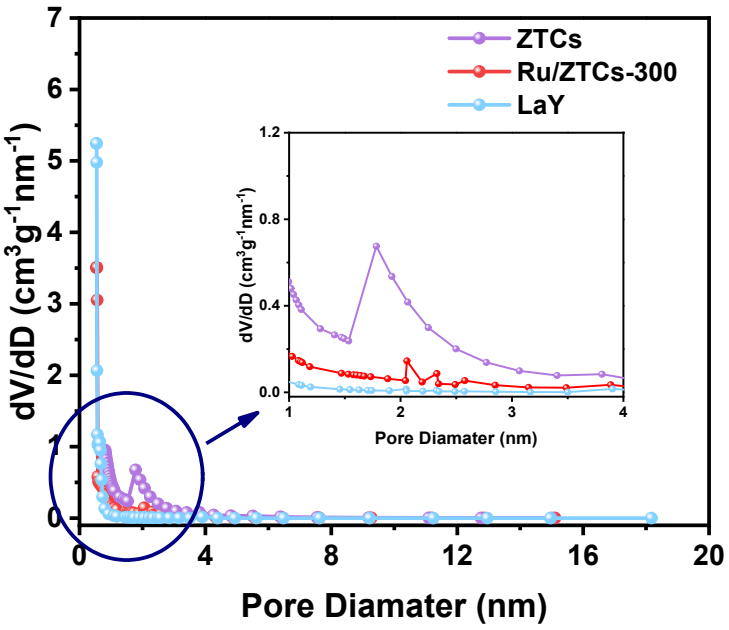

Figure S6. Pore size distribution of LaY, ZTCs and Ru/ZTCs-300.

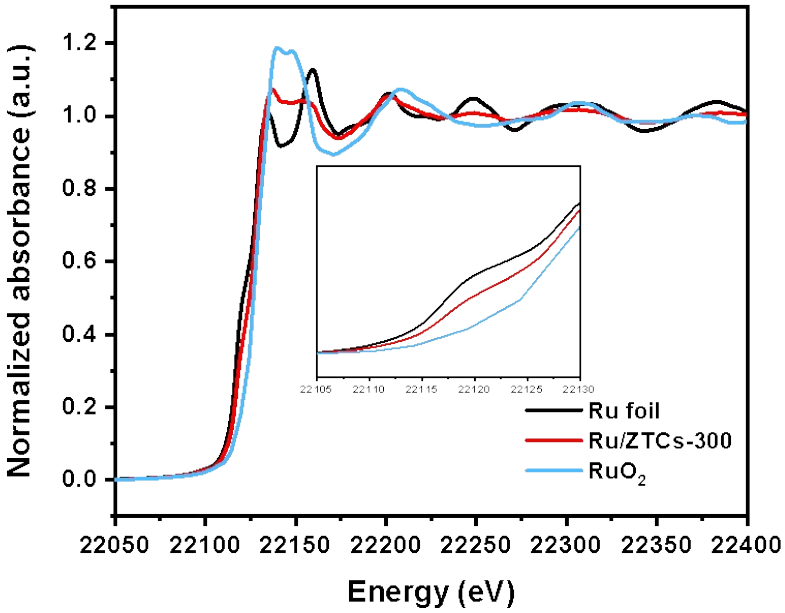

Figure S7. Normalized Ru K-edge XANES spectra and magnified pre-edge XANES region (inset).

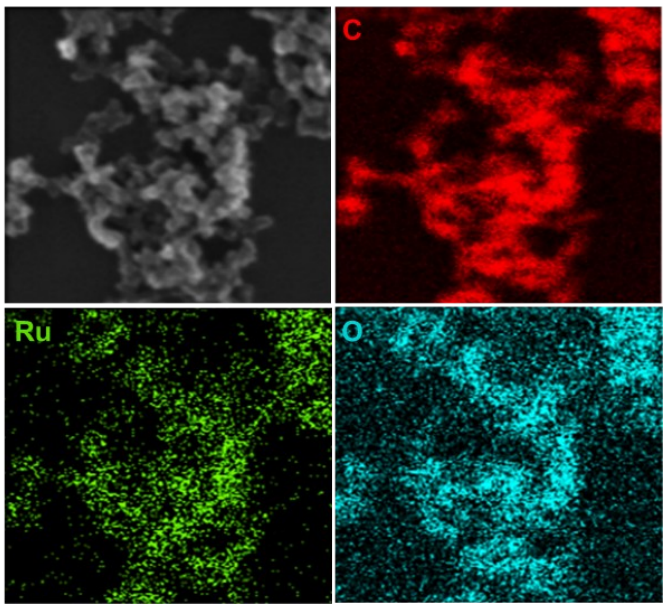

Figure S8. SEM and corresponding elemental mapping images of Ru/CB-300.

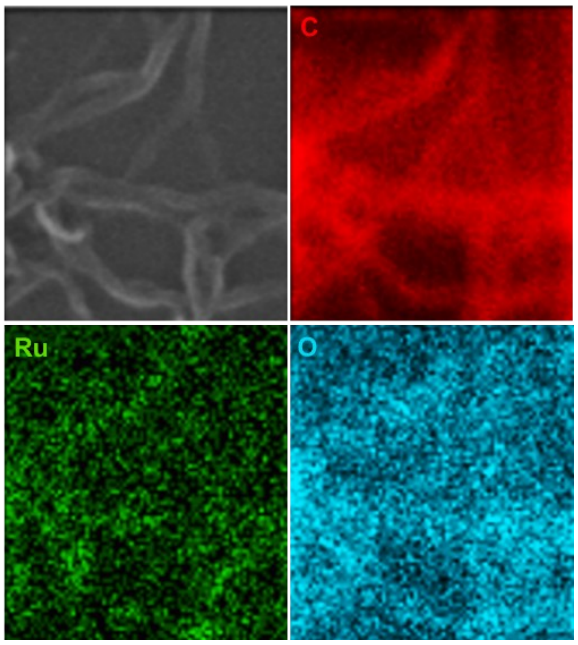

Figure S9. SEM and corresponding elemental mapping images of Ru/CNTs-300.

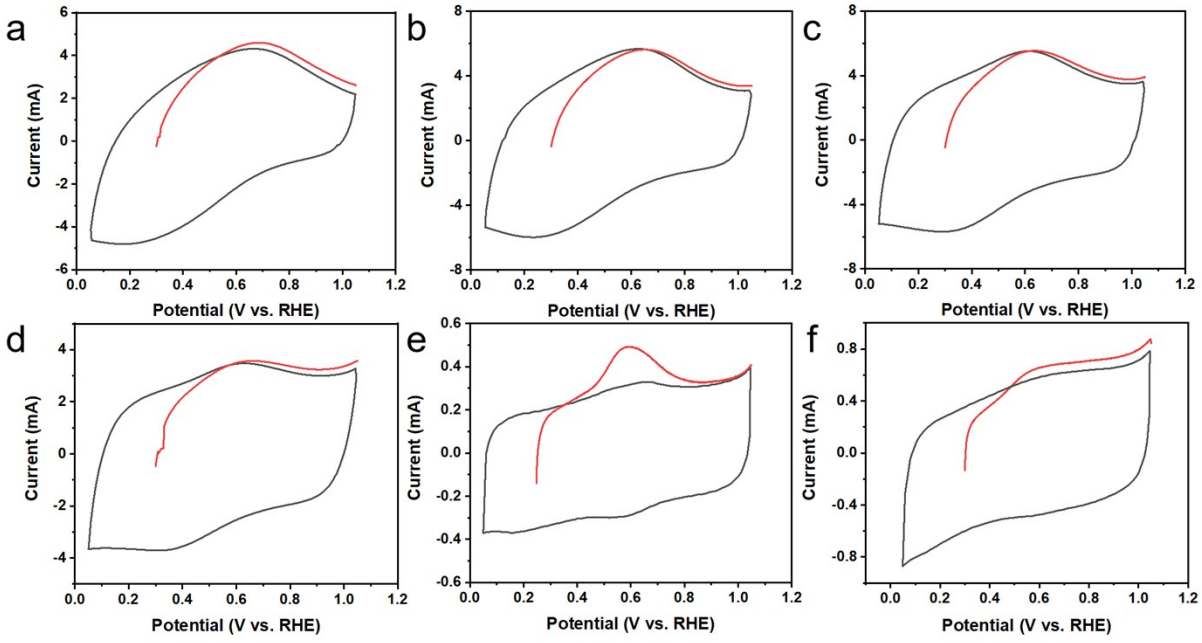

Figure S10. Copper UPD curves in 0.5 M H_2SO_4 in the absence and presence of 5mM $CuSO_4$ on (a)Ru/ZTCs-200, (b)Ru/ZTCs-300, (c)Ru/ZTCs-400, (d)Ru/ZTCs-500, (e)Ru/CNTs-300, (d)Ru/CB-300. The electrode was polarized at 0.3 V for 100 s to form the UPD layer.

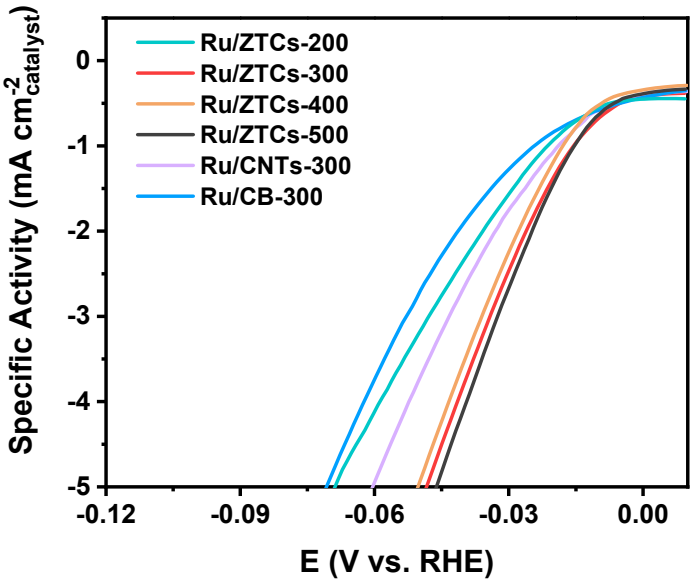

Figure S11. The specific activity of various catalysts.

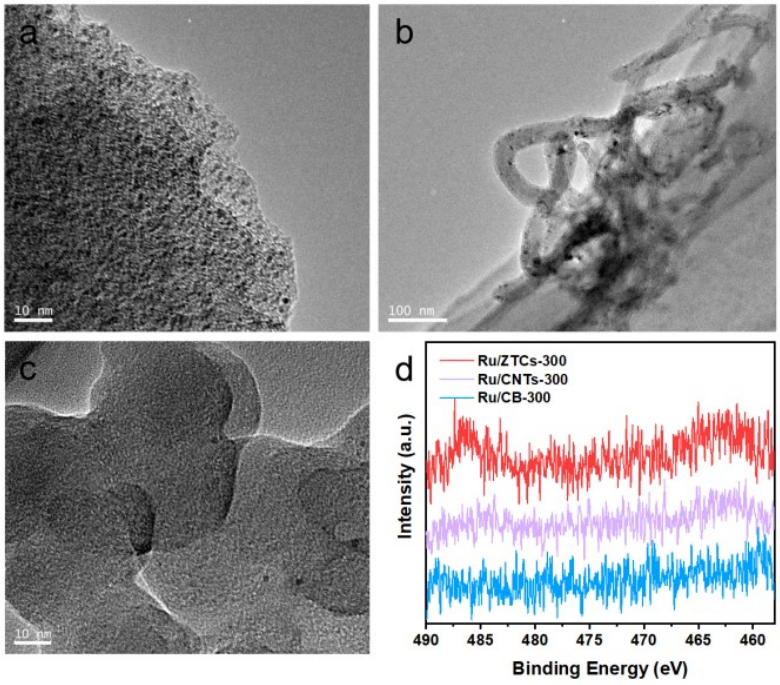

Figure S12. TEM images of (a)Ru/ZTCs-300, (b)Ru/CNTs-300 and (c)Ru/CB-300 after HER electrolysis. (d) Ru3p XPS spectrum of Ru/ZTCs-300, Ru/CNTs-300 and Ru/CB-300 after long-term stability tests in 1.0 M KOH.

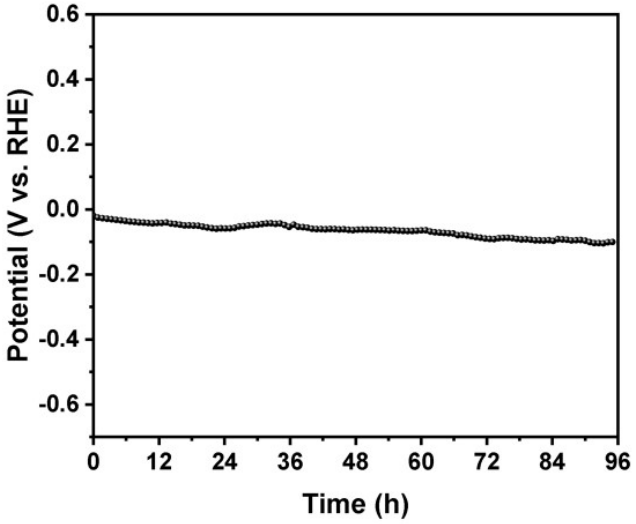

Figure S13. Test of long-term durability at a constant current density of 10 mA cm^{-2}.

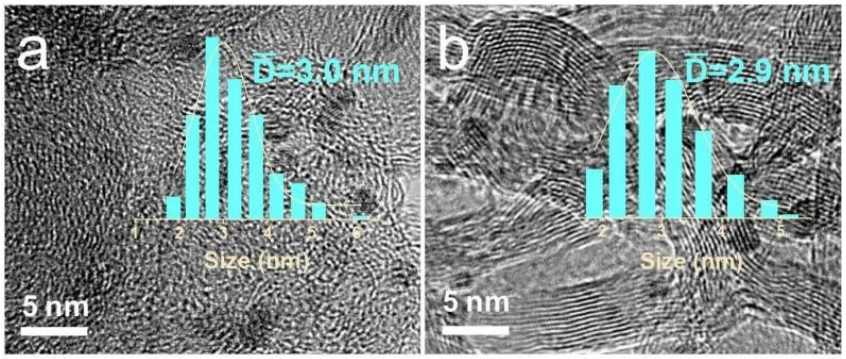

Figure S14. TEM images and particle size distributions of (a) Ru/CB-300, and (b) Ru/CNTs-300.

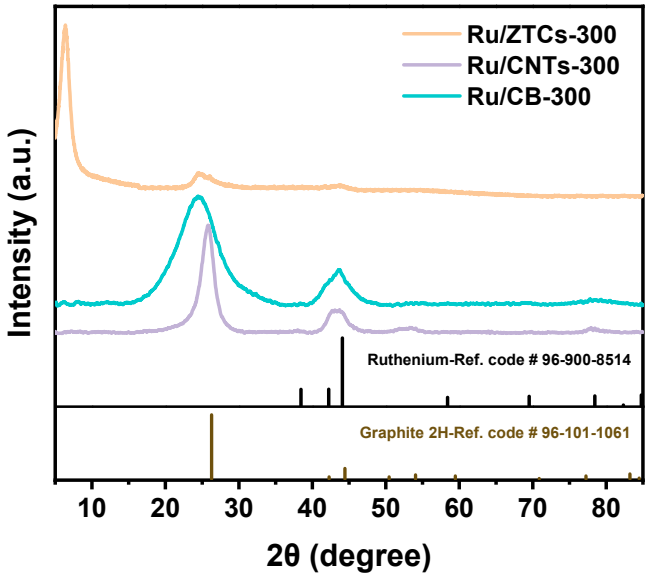

Figure S15. XRD patterns of Ru/ZTCs-300, Ru/CNTs-300, Ru/CB-300.

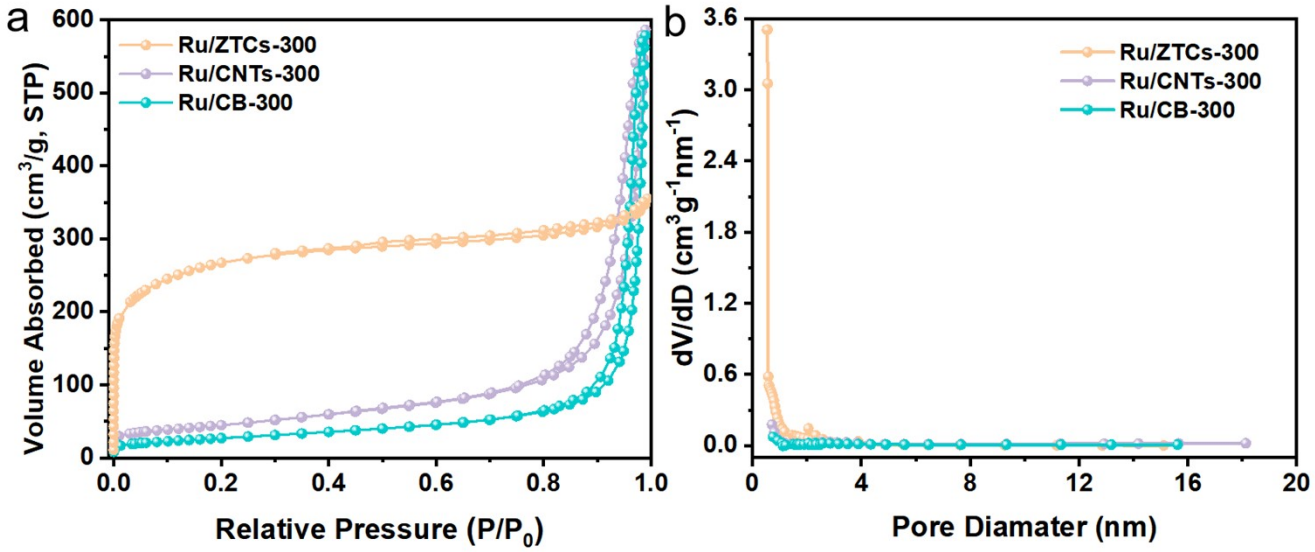

Figure S16. (a) N_2 adsorption-desorption isotherms and (b) pore size distribution of Ru/ZTCs-300, Ru/CNTs-300 and Ru/CB-300.

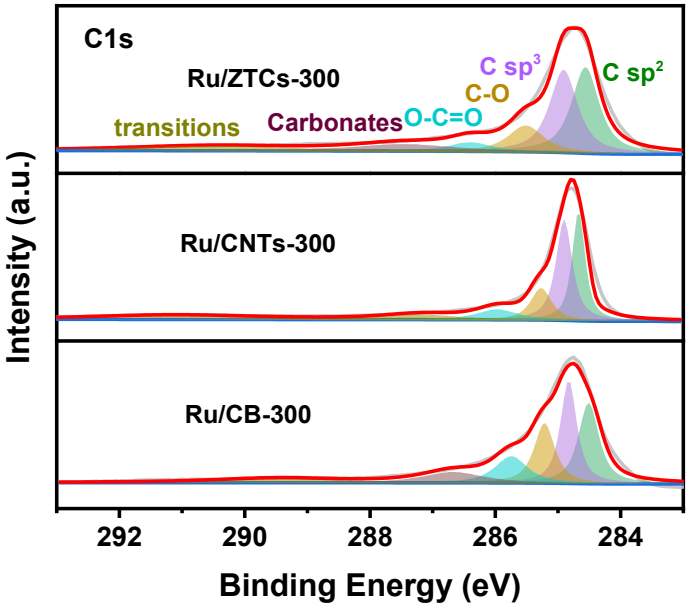

Figure S17. XPS spectra of C 1s for Ru/ZTCs-300, Ru/CNTs-300 and Ru/CB-300.

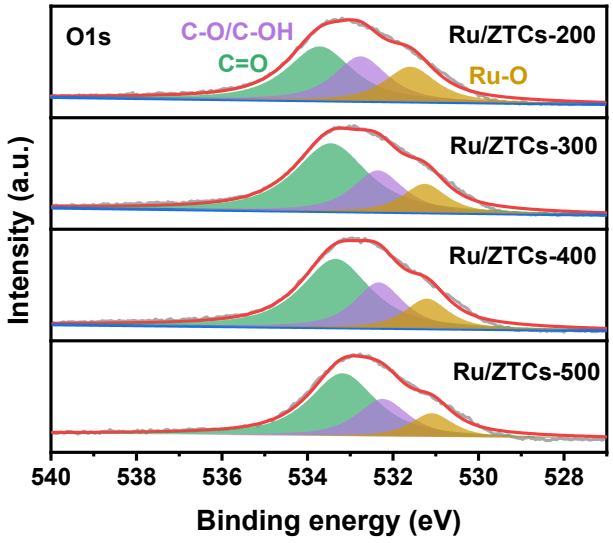

Figure S18. XPS spectra of O 1s for Ru/ZTCs-T samples.

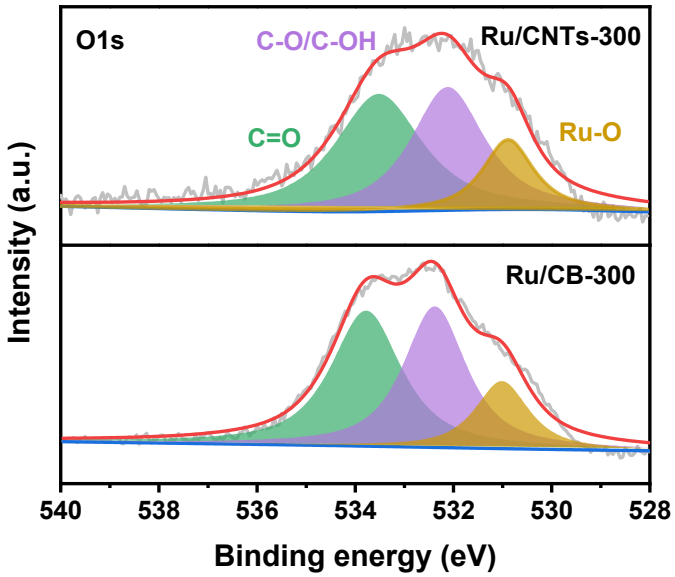

Figure S19. XPS spectra of O 1s for Ru/CNTs-300 and Ru/CB-300 samples.

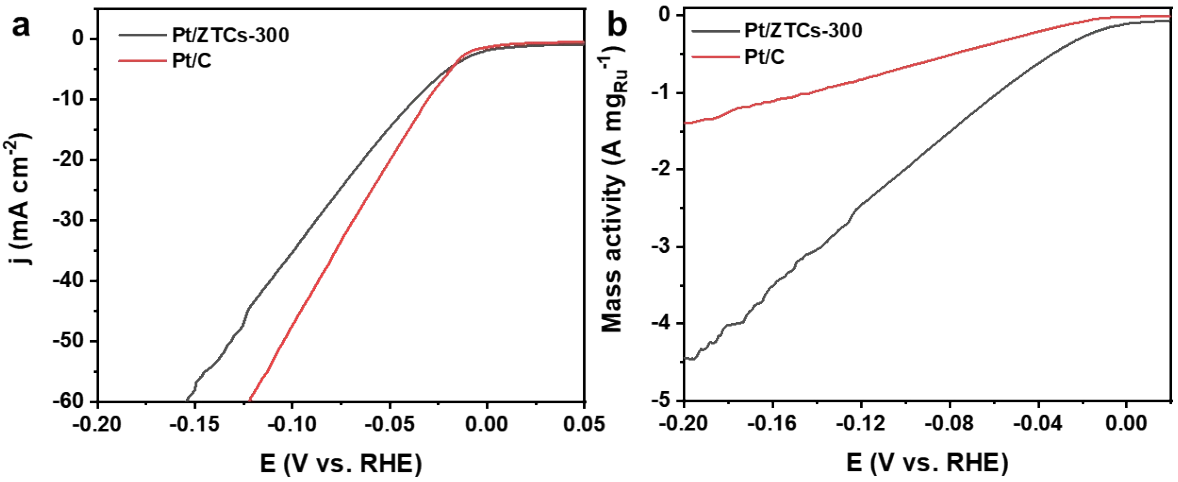

Figure S20. (a) HER polarization curves and (b) Mass activity of Pt/C and Pt/ZTCs-300.

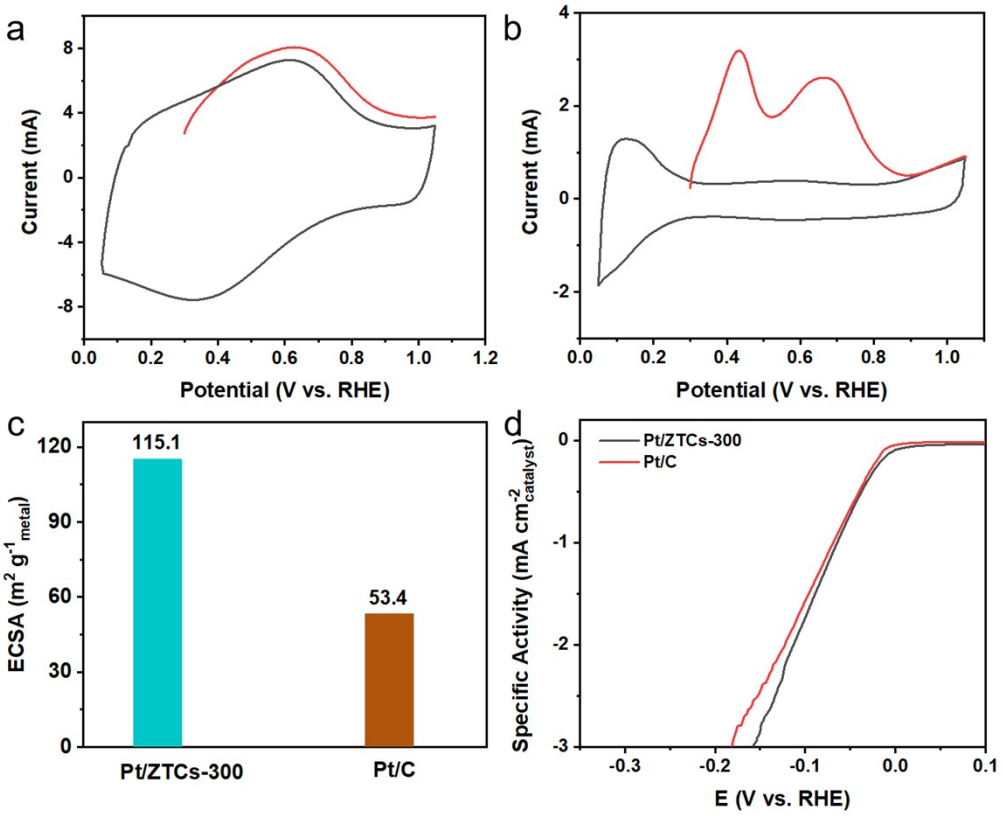

Figure S21. Copper UPD curves in 0.5 M H_2SO_4 in the absence and presence of 5mM $CuSO_4$ on (a)Pt/ZTCs-300, (b)Pt/C. The electrode was polarized at 0.215 V for 100 s to form the UPD layer. (c)The calculated ECSA for for Pt/ZTCs-300 and Pt/C by Cu UPD. (d) The specific activity of Pt/ZTCs-300 and Pt/C.

Supporting Tables

Table S1. Inductive Coupled Plasma Emission Spectrometer (ICP) results of prepared samples.

Sample	Ru (wt.%)	Pt (wt.%)
Ru/ZTCs-200	4.8	-
Ru/ZTCs-300	4.8	-
Ru/ZTCs-400	5.1	-
Ru/ZTCs-500	5.1	-
Ru/CNTs-300	4.9	-
Ru/CB-300	4.7	-
Pt/ZTCs-300	-	5.5

Table S2. Pore structural properties of LaY, ZTCs, Ru/ ZTCs, Ru/CNTs and Ru/CB.

Sample	S_{BET} ($m^2 \cdot g^{-1}$)[a]	S_{mi} t-plot ($m^2 \cdot g^{-1}$)	V_t ($cm^3 \cdot g^{-1}$)[b]	V_{mi} ($cm^3 \cdot g^{-1}$)v[c]	R_{mi}[d]
LaY	763	756	0.31	0.29	0.94
ZTCs	2162	1645	1.35	0.78	0.58
Ru/ZTCs-300	950	851	0.55	0.38	0.69
Ru/CNTs-300	156	1.42	0.91	$3.32*10^{-2}$	$3.65*10^{-2}$
Ru/CB-300	92	0.89	0.90	$2.73*10^{-2}$	$3.03*10^{-2}$

a BET-specific surface area was calculated from the adsorption branch in P/P_0 = 0.02–0.15.

b Total pore volume was determined at P/P_0 = 0.99.

c Micropore volume was calculated from the v-t plot at P/P_0 = 0.4–0.6.

d Ratio of micropore to total volumes.

Table S3. EXAFS fitting [a] parameters at the Ru K-edge for various samples.

Sample	Shell	CN	R (Å)	σ^2 (10^{-3} Å)	ΔE_0 (eV)	R factor
Ru/ZTCs-300	Ru- Ru	4.6	2.68	5.3	4.8	0.005
	Ru-O	3.9	1.99	9.6	4.2	
Ru foil	Ru- Ru	12.0	2.68	3.6	4.3	0.018
RuO_2	Ru-O	6.0	1.98	3.1	2.5	0.004

[a] CN, the coordination number for the absorber-backscatterer pair. R, the average absorber-backscatterer distance. σ^2, the Debye-Waller factor. ΔE_0, the inner potential correction. The accuracies of the above parameters were estimated as: N, ±20%; R, ±1%; σ^2, ±20%; ΔE_0, ±20%.

Table S4. The HER performance of Ru/ZTCs compared with other ruthenium-carbon composites in 1M KOH.

Electrocatalyst	j (mA cm^{-2})	η_j (mV)	Tafel slope (mV dec^{-1})	Ref.
Ru/ZTCs	10	26	39	This work
Ru/g-C_3N_4-C-TiO_2	10	107	85	1
Ru/C	10	186	125	2
Ru@CQDs-800	10	86	63	3
N-Ru-2/C	10	31	106	4
Ni@Ru/CNS-10%	10	20.1	87.3	5
Ru/OG	10	48	32.4	6
Ru@NPCH	10	35	37.9	7
Ru@WNO-C	10	24(100%iR)	39.7	8
Ru@CN	10	32	53	9
Ru@C_2N	10	17	38	10
Ru-MoS_2/CNT	10	50	62	11
s-RuS_2/S-rGO	10	25	29	12
Ru/3DNCN	10	17	42	13

Table S5. ICP results of dissolved content of Ru after long-term stability in different catalysts.

Sample	Ru (mg L^{-1})
Ru/ZTCs-300	0.014
Ru/CNTs-300	0.350
Ru/CB-300	0.741

Table S6. The area ratio of SP^2 to SP^3 of Ru/ZTCs, Ru/CNTs and Ru/CB measured by Raman Spectroscopy.

Sample	SP^2/SP^3 area ration
Ru/ZTCs-300	0.976
Ru/CNTs-300	1.187
Ru/CB-300	1.013

Table S7. The binding energy of Ru $3d_{5/2}$ of Ru/ZTCs samples measured by XPS.

Sample	Binding energy (eV)		$Ru^0/Ru^{\delta+}$
	$Ru^{\delta+}$	Ru^0	
Ru/ZTCs-200	465.8	463.1	1.03
Ru/ZTCs-300	465.8	463.1	1.36
Ru/ZTCs-400	465.8	462.9	1.48
Ru/ZTCs-500	465.8	463.0	1.82

Table S8. The area ratio of Ru-O of Ru/ZTCs samples measured by XPS.

Sample	Ru-O ration
Ru/ZTCs-200	0.233
Ru/ZTCs-300	0.153
Ru/ZTCs-400	0.146
Ru/ZTCs-500	0.142

Table S9. The binding energy of Ru $3d_{5/2}$ of Ru/ZTCs-300, Ru/CNTs-300 and Ru/CB-300 measured by XPS.

Sample	Binding energy (eV)		$Ru^0/Ru^{\delta+}$
	$Ru^{\delta+}$	Ru^0	
Ru/ZTCs	465.8	463.1	1.36
Ru/CNTs	465.8	463.1	2.48
Ru/CB	465.8	463.1	1.88

Table S10. The area ratio of Ru-O of Ru/ZTCs-300, Ru/CNTs-300 and Ru/CB-300 measured by XPS.

Sample	Ru-O ration
Ru/ZTCs-300	0.163
Ru/CNTs-300	0.136
Ru/CB-300	0.138

Table S11. H_2 chemisorption results for different Ru/ZTCs-T samples.

Sample	H_2 uptake ($\mu mol_{H2}\ g_{catalyst}^{-1}$)
Ru/ZTCs-200	24.68
Ru/ZTCs-300	28.86
Ru/ZTCs-400	32.42
Ru/ZTCs-500	36.01

References

1. Z. L. Li, Y. Yang, S. X. Wang, L. Gu and S. Shao, *ACS Appl. Mater. Interfaces*, 2021, **13**, 46608-46619.

2. Y. J. Wang, J. K. Wang, T. P. Xie, Q. Y. Zhu, D. Zeng, R. Li, X. D. Zhang and S. L. Liu, *Appl. Surf. Sci.*, 2019, **485**, 506-512.

3. W. D. Li, Z. H. Wei, B. Y. Wang, Y. Liu, H. Q. Song, Z. Y. Tang, B. Yang and S. Y. Lu, *Mater. Chem. Front.*, 2020, **4**, 277.

4. Y. M. Zhao, X. W. Wang, Z. Li, P. P. Zhao, C. L. Tao, G. Z. Cheng and W. Luo, *Chinese Chem. Lett.*, 2022, **33**, 1065–1069.

5. W. Wu, Y. Wu, D. Zheng, K. Wang and Z. h. Tang, *Electrochimica Acta*, 2019, **320**, 34568.

6. P. P. Su, W. Pei, X. W. Wang, Y. F. Ma, Q. K. Jiang, J. Liang, S. Zhou, J. J. Zhao, J. Liu and G. Q. (Max) Lu, *Angew. Chem.* 2021, **133**, 16180-16186.

7. J. Tang, B. Wang, Y. Z. Zhang, X. H. Zhang, Q. H. Shen, J. F. Qin, S. Xue, X. Guo, C. C. Du and J. H. Chen, *J. Mater. Chem. A*, 2022, **10**, 4181-4190.

8. G. Meng, H. Tian, L. X. Peng, Z. H. Ma, Y. F. Chen, C. Chen, Z. W. Chang, X. Z. Cui and J. L. Shi, *Nano Energy*, 2021, **80**, 105531.

9. J. Wang, Z. Z. Wei, S. J. Mao, H. R. Li and Y. Wang, *Energy Environ. Sci.*, 2018, **11**, 800-806.

10. J. Mahmood, F. Li, S. M. Jung, M. S. Okyay, I. Ahmad, S. J. Kim, N. Park, H. Y. Jeong and J. B. Baek, *Nat. Nanotechnol.*, 2017, **12**, 441-446.

11. X. Zhang, F. Zhou, S. Zhang, Y. Y. Liang and R. H. Wang, *Adv. Sci.*, 2019, **6**, 1900090.

12. J. Yu, Y. N. Guo, S. S. Miao, M. Ni, W. Zhou and Z. P. Shao, *ACS Appl. Mater. Interfaces*, 2018, **10**, 40, 34098.

13. H. Li, M. T. Zhang, L. C. Yi, Y. J. Liu, K. Chen, P. Shao and Z. H. Wen, *Appl. Catal. B*, 2021, **280**, 119412